JOURNAL OF CATALYSIS, 99, 472–481 (1986)

Effects of Particle Structure on CO Hydrogenation on Ni on SiO_2[1]

C. LEE,* L. D. SCHMIDT,* J. F. MOULDER,† AND T. W. RUSCH†

*Department of Chemical Engineering and Materials Science, University of Minnesota, Minneapolis, Minnesota 55455; and †Physical Electronics Division, Perkin–Elmer, Eden Prairie, Minnesota 55344

Received June 18, 1985; revised January 23, 1986

The effects of oxidation–reduction cycling on the morphology, surface composition, hydrogen uptake, and kinetics of CO hydrogenation over silica-supported Ni catalysts have been studied by hydrogen chemisorption, kinetics in a differential flow reactor, transmission electron microscopy (TEM), and X-ray photoelectron spectroscopy (XPS) in a rapid transfer reactor system. When Ni particles (~4% dispersion, ~250 Å diameter) are oxidized at 460°C and then reduced in H_2 at 300°C, hydrogen chemisorption areas increase while methanation activities decrease. Heating progressively up to 650°C produces a decrease in surface area and an increase in methanation activity. XPS confirms total oxidation and reduction of Ni by 350°C. TEM shows that particles spread on the SiO_2 surface upon oxidation and form clusters of smaller Ni particles upon low-temperature reduction. These results show that solid-state redispersion occurs upon oxidation–reduction cycling but that the methanation activity is low on freshly reduced Ni. It is argued that the activity change is caused by a lower activity on high index planes of smaller particles of Ni which may be associated with preferential buildup of carbon on these planes. These transformations can be produced reversibly on fairly large particles, and these structures can be metastable for long times under reaction conditions.

INTRODUCTION

Nickel catalysts find widespread application in hydrogenation, hydrotreating, and steam reforming reactions. Considerable recent interest has centered on nickel catalysts for methanation of coal synthesis gas. Commercial catalysts are typically nickel particles dispersed on oxide supports such as Al_2O_3 or SiO_2. In the past 10 years, the hydrogenation of carbon monoxide over transition metal catalysts has been widely studied, and thorough reviews (*1–6*) have discussed various aspects of this reaction on catalysts from single crystals (*1, 2*) to high dispersion particles on high-area oxide supports (*3–5*).

Supported metal catalysts are exposed to various oxidizing and reducing gas atmospheres during their preparation, operation, and regeneration. The microstructure of small particles can be altered by different gas environments, and this may play an important role in determining the performance of the catalyst. On the other hand, heterogeneous reactions take place only on the top monolayer of the particle surface, and it is therefore necessary to characterize the structure of small particles and correlate the reactivity of the catalyst with its morphology and surface composition. This characterization can only be obtained with electron microscopy coupled with surface sensitive spectroscopies.

Recently, transmission electron microscopy (TEM) studies using model catalysts have revealed various types of the behavior of supported metal particles in gaseous environments (*7–11*). One interesting finding is that alternate oxidation and reduction can lead to an increase in surface area of supported particles, i.e., redispersion. Previously, we observed the redispersion of rhodium on silica and alumina (*10*). Nakayama *et al.* (*11*) have shown that silica- and alumina-supported nickel particles can be redispersed by repeated oxidation–reduction treatments.

[1] This work partially supported by NSF under Grant CPE 821408.

0021-9517/86 $3.00

The influence of dispersion on the performance of supported Group VIII metals for the CO hydrogenation reaction has been studied by several research groups. Vannice (*12*) has reported that the specific activity for methanation on Pt and Pd catalysts increases with increasing dispersion, while Bartholomew *et al.* (*13*) found that the methanation activity of Ni catalysts decreases with increasing dispersion. Dalla Betta *et al.* (*14*), King (*15*), and Kellner and Bell (*16*) observed a similar trend (decreasing activity with increasing dispersion) for Ru catalysts.

The present study aims to elucidate the correlation between particle microstructure and kinetics by examining the effects of repeated oxidation–reduction on the performance of Ni particles on amorphous SiO_2. We examine the same catalysts before and after various gas and heat treatments to follow the morphological changes. We show, using TEM, that reduction of NiO produces breakup into clusters of small metal particles. The effects of redispersion on activity is correlated with hydrogen uptake and CO hydrogenation kinetics measured in a differential flow reactor.

It has become customary to assume that properties of catalyst particles should correlate with dispersion (the fraction of surface metal atoms). This appears to originate from the work of van Hardeveld and Hartog (*17*) who calculated fractions of edge and corner atoms on polyhedra as a function of particle size. We note that dispersion is related only tenuously to microstructure, because the model of these workers assumes that all particles are single-crystal polyhedra.

EXPERIMENTAL

A flow microreactor system and an online HP 5793 gas chromatograph (GC) were used to study hydrogen chemisorption and CO hydrogenation kinetics. Catalyst samples weighing about 300 mg were used in the microreactor. Hydrogen uptake was measured by the GC flow desorption method described by Butt *et al.* (*18*) using a thermal conductivity detector (TCD). In the flow desorption method the catalyst was cooled in H_2 from the reduction temperature to 0°C by removing the oven and letting the reactor cool in air for 5 min before immersion in an ice bath for 20 min. The reactor was then purged with nitrogen at 0°C and subsequently heated to 400°C for 15 min. Finally, a valve was switched to allow the desorption pulse to pass to the TCD. The reactor response was calibrated after each experiment by injecting several 225-μl pulses of H_2. The most convincing justification for the accuracy of this technique is the agreement of the specific activities of catalysts used in this study with the literature data shown in Table 1.

For kinetic measurements the conversion of CO was kept less than 5%. The activity and product distribution were analyzed by the GC using a flame ionization detector (FID).

The 15% Ni/SiO_2 catalyst was prepared by impregnation of Cab-O-Sil SiO_2 with a surface area of 200 m^2/g to incipient wetness with an aqueous solution of $Ni(NO)_3$. After impregnation, the catalyst was dried overnight at 100°C and then calcined in air at 300°C for 10 h. Catalyst samples of about 125 mg were pressed into 13-mm-diameter disks for XPS studies. Hydrogen (99.9995%, Matheson) was purified by a liquid-nitrogen trap. The reaction gas mixture (25% CO in H_2, Linde) was passed through a molecular sieve trap to remove carbonyls.

TABLE 1

Comparison of CO + H_2 Reaction Rates Extrapolated to 258°C over Ni/SiO_2 Catalysts

Investigator	Loading	TOF × 10^3 sec^{-1}
Vannice (*19*)	17%	13.9
Vannice (*19*)	17%	19.9
Butt *et al.* (*18*)	—	11.6
Goodman *et al.* (*20*)[a]	(100) and (111) crystals	20.0
Bartholomew *et al.* (*13*)[a]	15%	5.2
This study	15%	9.6 to 27.8

[a] Used 4 : 1 H_2/CO ratio, otherwise used 3 : 1 H_2/CO ratio.

High-purity air containing <2.0 ppm total hydrocarbons as CH_4 was used without further purification. Nitrogen carrier gas (zero gas, Matheson) for hydrogen chemisorption experiments was passed through an Oxisorb unit to remove traces of oxygen.

Planar samples for TEM were prepared by vacuum deposition of a 15- to 20-Å Ni film on a 200-Å-thick SiO_2 flake mounted on a gold grid using procedures described previously (*10*). The SiO_2 substrate was prepared by vacuum deposition of a 300-Å-thick film of Si on NaCl, floating Si flakes off in H_2O, catching a flake on a gold grid, and oxidizing to 800°C in air for several days. The SiO_2 formed by this procedure was planar and completely amorphous. TEM samples were treated in a quartz tube furnace in flowing gases. Samples were examined in a JEOL JEM-100CX STEM. A sample could be transferred repeatedly between the STEM and quartz tube furnace so that morphological changes of individual particles could be examined.

The most difficult aspect of analyzing oxidation states of samples by XPS is the presence of surface contamination and oxidation which occur after removal from the reaction environment. The capability for transferring the sample from a reactor to the UHV chamber under vacuum is therefore essential. The surface composition change during oxidation–reduction was monitored by XPS with an appended reaction chamber which facilitates sample transfer under vacuum. For XPS studies, a Perkin–Elmer Physical Electronics Model 2650 reactor system was attached to a PHI Model 5300 ESCA system via a manually operated gate valve. The reaction chamber was made by machining a small volume cavity into a stainless-steel block which was mounted on a six-way cross with the cavity opening facing the interior of the six-way cross. A movable cap on which the sample was mounted sealed the cavity. For XPS analysis the reaction chamber was opened and the reactor pumped down to 10^{-7} Torr in 5 min with a turbomolecular pump. The reactor was equipped with a linear transport attachment to transfer the sample between the reaction chamber and UHV spectrometer under vacuum. Samples could be heated in the reaction chamber at temperatures up to 600°C by heating the reactor walls using cartridge heaters. Reactive gases were passed over the heated sample with the reaction chamber isolated from the turbomolecular pump. At different treatment stages, the reactor was opened, the sample transferred into the spectrometer, and XPS spectra recorded. XPS spectra were taken with a Mg$K\alpha$ anode using a 180° sector spherical capacitor analyzer. Peak energies were calibrated against Si (103.4 eV) and C (284.6 eV) peaks.

RESULTS

Activity and Surface Area

To investigate the effects of cyclic oxidation–reduction on CO hydrogenation kinetics, the catalyst in the Pyrex reactor was subjected to the same treatment used for TEM and XPS studies. After each stage of reduction or oxidation–reduction, the sample was brought to the desired temperature in flowing H_2 (~40 cm^3/min), the reactant mixture in a 3 : 1 H_2/CO ratio and a total pressure of 1 atm was introduced into the reactor at ~60 cm^3/min, and the effluent concentrations were monitored as a function of time. At all temperatures a transient decrease in the conversion and CH_4 formation occurred for about 120 min until a steady-state activity was obtained. In results soon to be published we will show that this initial activity decrease is accompanied by buildup of monolayers of carbon on the surface as measured by XPS.

Figure 1 shows the steady-state methane production rate as a function of temperature after each stage of treatment. The activity is lower with 300°C reduction than after 350°C reduction. Moreover, the activation energy with 300°C reduction is 26.6 kcal/mol which is 2.3 kcal/mol higher than that after 350°C reduction. There is no dif-

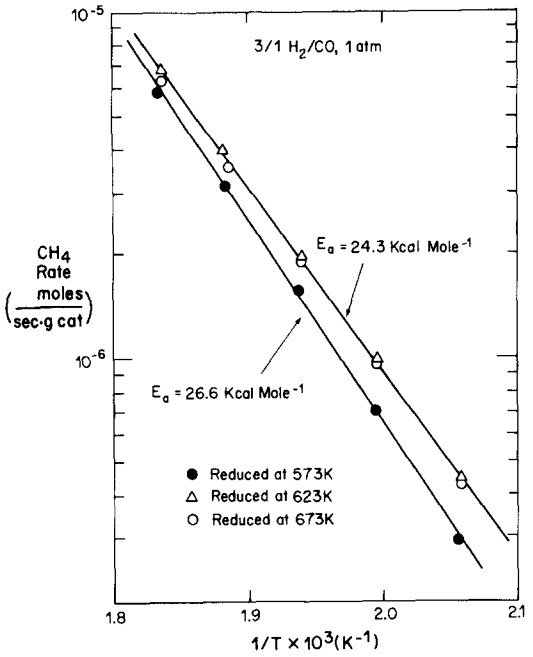

FIG. 1. Arrhenius plot for steady-state methane formation over a 15% Ni/SiO_2 catalyst, (a) after 300°C reduction and (b) after 350 and 400°C reduction.

ference in activity or activation energy between 350 and 400°C reduction in H_2. The activation energy of 24.3 kcal/mol obtained with reduction temperature higher than 350°C is in good agreement with the activation energy of 24.7 kcal/mol measured for (100) oriented Ni single-crystal catalysts (e.g., Goodman (*20*).

The hydrogen uptake and methanation rate as a function of repeated oxidation–reduction treatments are shown in Fig. 2. The abscissa is the total reduction time beginning with the freshly calcined sample. After each treatment, the activity (H_2/CO = 3 : 1, 1 atm, 258°C) and hydrogen uptake were measured, and corresponding points in Fig. 2 represent these results. The difference in total reduction time between a particular point and the one before gives the reduction time of that treatment. Reduction temperatures are specified next to each data point. For each oxidation–reduction, the sample was oxidized in flowing air at 460°C for 10 h and then reduced in H_2 for another 10 h. Each oxidation–reduction is indicated by an O_2 and an arrow next to the line between those points.

As shown in Fig. 2a, sintering at increasing temperatures and longer times correlates with a decrease of hydrogen uptake, while redispersion by oxidation–reduction increases the amount of hydrogen uptake. These are the expected results: the surface area decreases due to sintering at higher temperatures and longer reduction time, while redispersion of Ni particles by oxidation–reduction treatments increases the surface area.

However, the methanation activity variation is opposite to the chemisorption area. As shown in Fig. 2b, a significant loss of

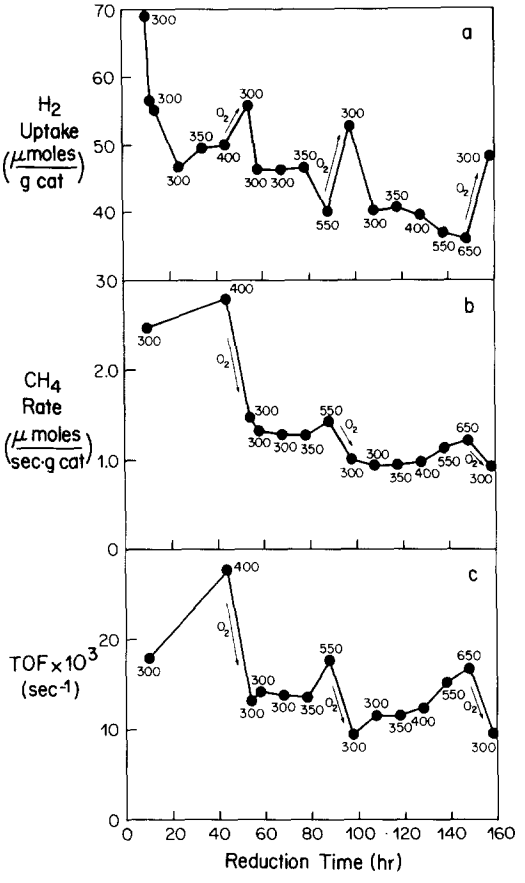

FIG. 2. Effects of different treatments on the performance of a 15% Ni/SiO_2 catalyst, (a) hydrogen uptake, (b) methanation activity, and (c) turnover frequency vs reduction time. The activities were measured at 258°C with a H_2 : CO ratio of 3 : 1 at 1 atm.

activity is observed after each oxidation-reduction treatment, but the activity recovers upon continued H_2 treatment at higher temperatures. Thus high dispersion correlates with lower activity. This agrees with Bartholomew's results (*13*) obtained from many samples with different dispersions. The turnover frequency is computed by dividing the activity by the amount of hydrogen uptake (Fig. 2c), and follows the same trend as the activity except with a larger variation in amplitude.

Microstructures

The morphology change of supported Ni particles during cyclic oxidation–reduction was studied using planar samples treated identically to the porous supported samples. These samples were transferred repeatedly between the STEM and the quartz tube furnace to examine the same Ni particles before and after various treatments.

Samples were exposed to laboratory air at room temperature between treatment and analysis by TEM or XPS. This produced a thin layer of $Ni(OH)_2$ and NiO as shown by XPS. However, samples still had strong Ni metal XPS peaks after air exposure which indicates that the oxidized layers were only a few Ångstroms thick. TEM also shows that these oxide layers must have been very thin because air treatment for several hours at 200°C produced oxide layers only 10–20 Å in thickness.

Figures 3a and b show micrographs of a specimen with an 18-Å initial loading of pure Ni metal film on amorphous SiO_2 after heating successively in flowing H_2 at 650°C and then in air at 460°C for 2 h. At 460°C in air, crystallites with initial diameters in the range of 50 to 250 Å spread over the surface of the substrate. The diffraction pattern indicates that after this treatment most of the Ni is oxidized to NiO, leaving only a small amount of higher contrast unoxidized metal at the core of most oxide particles. This result resembles those from experiments described previously for oxidation–reduction of Rh on SiO_2 (*10*).

Figures 3c through 3h show micrographs of the same region following exposures to H_2 for 2 h at successively increasing temperatures. Upon reduction at 300°C (Fig. 3c) a dramatic change in morphology takes place. The oxide particles split into many small clusters. Electron diffraction at this temperature showed a diffuse fcc ring pattern mixed with a very weak oxide pattern, indicating that these small clusters are mostly reduced but not well crystallized. This splitting phenomena seems to occur for particles of all sizes.

Comparison of this micrograph with Fig. 3a shows that each original particle breaks into a cluster of much smaller particles (~30 Å), and the shapes of these clusters are irregular. Heating at 350°C results in only a slight difference in appearance (Figs. 3c and d). However the electron diffraction pattern at 350°C shows only sharp rings of fcc metal.

Subsequent heating of this sample to higher temperatures in H_2 produces sintering and coalescence of Ni crystallites. Figures 3e through h show micrographs of the same region at 450, 550, 650, and 750°C, respectively. Coalescence occurs by growth of larger particles which finally merge with nearby particles.

Oxidation States

To calibrate XPS peak positions and intensities, and to observe surface oxidation during transfer in air, a Ni foil was cleaned by argon ion sputtering to remove surface oxides and then removed from the XPS chamber for different time periods at room temperature. The sample was transferred to spectrometer for surface analysis after each air exposure. The binding energy of metallic Ni $2p_{2/3}$ (curve a in Fig. 4A) was 852.6 eV, in agreement with literature values (*21*). After 1 min air exposure as shown in Fig. 4b, several new peaks grew in. The Ni $2p$ and shakeup peaks provide information about the chemical forms on the surface. The new peak at 856 eV and the shakeup peak at 861 eV are assigned as Ni^{2+} in

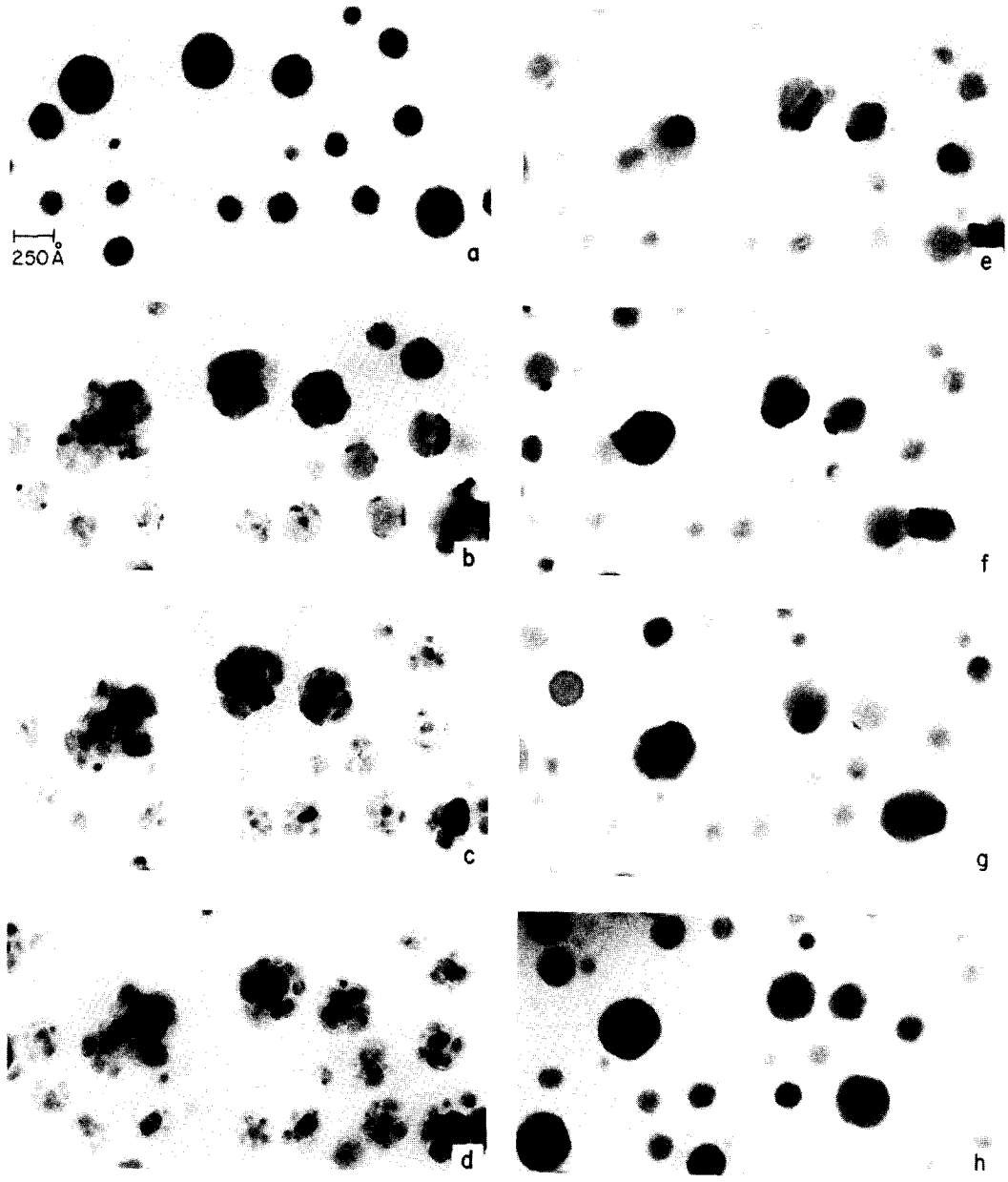

FIG. 3. Transmission electron micrographs showing the morphologies of metal and oxide particles formed by heating pure Ni on SiO_2 for 2 h in (a) H_2 at 650°C and (b) air at 460°C. This was followed by heating in H_2 at (c) 300°C, (d) 350°C, (e) 450°C, (f) 550°C, (g) 650°C, and (h) 750°C, respectively. Splitting of metal particles can be obtained by reducing NiO at low temperatures.

$Ni(OH)_2$. NiO and $Ni(OH)_2$ have similar Ni $2p$ binding energies and peak shapes.

In order to make an unambiguous identification of a particular compound, other core levels must be examined, particularly the oxygen $1s$ peak. As shown in Fig. 4B, the O $1s$ peak at 531.2 eV is attributed to $Ni(OH)_2$ and the shoulder at 529.6 eV is NiO. These are confirmed by studies on standard Ni compounds (*22*). We infer therefore that the Ni surface after air exposure was covered by $Ni(OH)_2$ with a small amount of NiO. When the exposure time was increased, the XPS spectra in Fig. 4A from

curve b to d show that Ni^{2+} peaks increase and Ni metal peaks decrease. For comparison, the XPS spectrum obtained with a 15% Ni/SiO_2 sample reduced in H_2 at 400°C and transferred in air to the UHV chamber is shown in curve e which is identical to curve d.

The 15% Ni/SiO_2 catalyst disks were first calcined in flowing air in the reactor at 300°C and then reduced in flowing H_2 at atmospheric pressure. After each stage of treatment, the sample was transferred back to the spectrometer under vacuum for surface analysis.

Figures 5A and B show high-resolution scans of Ni 2*p* and O 1*s* peaks for a succession of temperature and gas treatments. Heating in air at 300°C (curve a in Fig. 5A), produces predominantly NiO with Ni $2p_{2/3}$ at 855.2 eV and the characteristic lineshape of nickel oxide. This assignment is confirmed by the O 1*s* spectra in Fig. 5B.

Curving fitting was used to separate the contributions from the oxygen of the silica support at 532.6 eV and oxygen at 529.6 eV of NiO. Upon heating in H_2 at 300 and 350°C, curves b and c in Fig. 5A show that the oxide peaks decrease and metal peaks increase until at 350°C only metallic Ni peaks remain. Spectra in Fig. 5B also show the same trend in O 1*s* peaks. The relative amount of oxygen from NiO decreases with sequential H_2 reduction (Fig. 5B). There is no oxygen from NiO observed after reduction in H_2 at 350°C (curve c in Fig. 5B) just as on the Ni foil (curve a in Fig. 4A). The sample was then reoxidized at 460°C in flowing air and reduced at 300 and 350°C. The results are the same, as shown in Figs. 5A and B.

DISCUSSION

Redispersion has major consequences in supported metal catalysts, since it influences the shape and size distribution of metal crystallites which in turn can affect

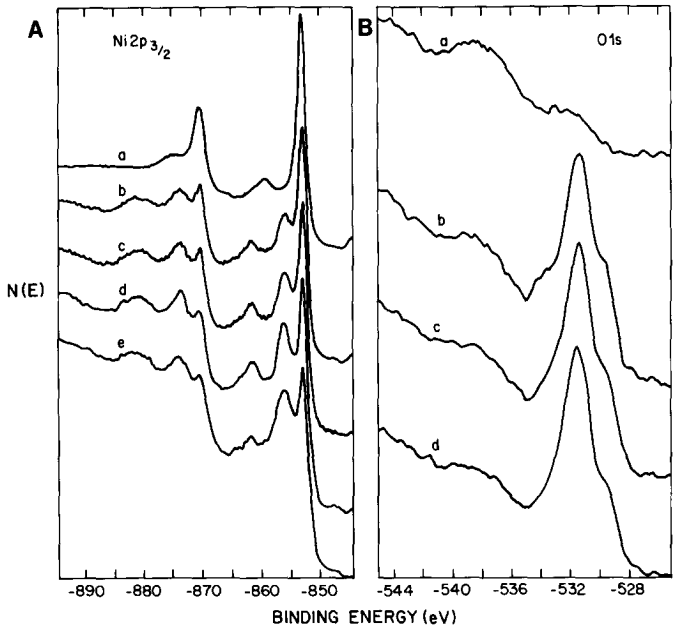

FIG. 4. (A) High-resolution XPS spectra of the Ni 2*p* peaks from Ni foil and Ni particles supported on SiO_2. Spectra were obtained after (a) sputter cleaning followed by air exposure at room temperature for (b) 1 min, (c) 15 min, and (d) 3 days. For comparison curve (e) is the surface oxidation of a Ni/SiO_2 sample transferred in air after 400°C reduction in H_2. (B) XPS spectra of the O 1*s* level from a Ni foil. The sample was (a) sputter-cleaned, then exposed to air sequentially for (b) 1 min, (c) 5 min, and (d) 3 days.

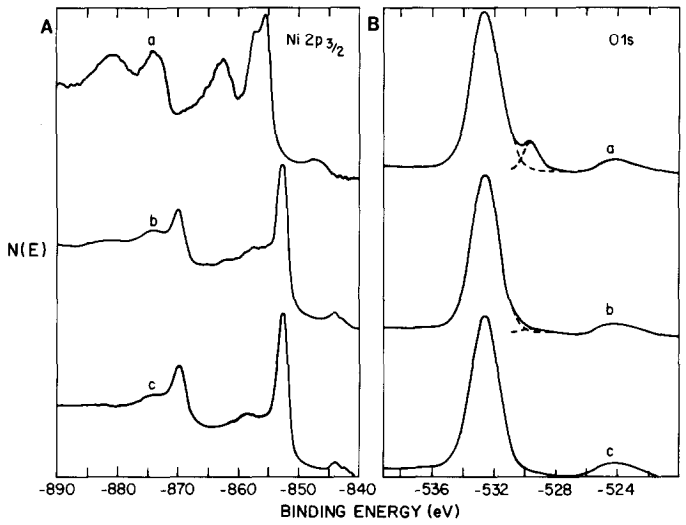

FIG. 5. (A) High-resolution XPS spectra of Ni 2*p* peaks from a 15% Ni/SiO_2 sample. Spectra were obtained after treatment sequentially (a) in air at 300°C, (b) in H_2 at 300°C, (c) in H_2 at 350°C and above. (B). XPS spectra of the O 1*s* level from a 15% Ni/SiO_2 sample. The sample was treated sequentially (a) in air at 300°C, (b) in H_2 at 300°C, (c) in H_2 at 350°C and above.

the kinetics. However, most studies have centered on either TEM studies of model systems or hydrogen chemisorption and kinetics measurement on high-area catalysts. There have been few studies attempting to correlate structure with catalyst performance, or to examine changes on the same catalyst. We shall first consider the mechanism of carbon deposition under CO hydrogenation conditions, then the anisotropy of carbon deposition on different crystallographic planes, and finally the correlation between redispersion and kinetics.

Effects of Carbon Deposition on Reaction Rate

The formation of carbon layers on metal surfaces during CO hydrogenation has been reported by several research groups. Goodman and co-workers (*20*) demonstrated that the active form of carbon on a nickel surface is carbidic in nature and can be readily hydrogenated, while graphite is a poison which blocks the active sites and deactivates surface. Bonzel and Krebs (*23*) found similar results for iron. Somorjai *et al.* (*24*) observed carbon deposition on Fe and Rh with Auger Electron Spectroscopy (AES). The general mechanism which has been proposed from these studies suggests that carbon monoxide and hydrogen are dissociatively adsorbed on the metal surface and that oxygen is rapidly removed through reaction with hydrogen to produce water. The active carbon may either react with other surface carbon to form graphite or react with hydrogen atoms and polymerize into hydrocarbons. This model explains the poisoning effect of graphite and also suggests that a competition for surface carbon between graphite deposition and hydrogenation to hydrocarbons results in the induction period observed over the 15% Ni/SiO_2 catalysts of this study.

Crystallographic Anisotropies in Carbon Formation on Nickel

Since reactions take place only on the top monolayer of the particle surface, crystallographic anisotropies should play an important role in determining the performance of catalysts. It has been shown (*25*) that the presence of kinks and steps increase the ability of CO dissociation on Ni surfaces. As mentioned previously this step is crucial in CO hydrogenation. Gwathmey and Cun-

ningham (*26*) examined large Ni single spheres following their exposure to gases at atmospheric pressure. Ethylene at 700 K produced a heavy black deposit on the Ni sphere. The (100) and (111) poles remained shiny, but the heaviest deposition was noted on the vicinal planes of (100).

Recently, Caracciolo and Schmidt (*27*) used a curved nickel single crystal which exposed the [100]–[111]–[110] zone to study crystallographic variations in the formation of surface carbon under methanation conditions. They reported that the carbon deposited from CO hydrogenation (H_2/CO = 3:1, 2 Torr, 600 K, 10 min) showed a very large anisotropy which is quite different from the anisotropy of C in C_2H_4 decomposition (*27*). The carbon level was significantly lower on the low index planes but much higher on the high index planes. The maximum amount of carbon was built up on (911), 15° away from (100) in the [100]–[111] zone.

van Hardeveld and Hartog (*17*) have calculated the surface sites distribution of fcc metal single crystals. For small single crystals, corner and edge atoms are a significant fraction of the total surface atoms, while larger particles (>100 Å) consist predominantly of the low free energy (111) and (100) planes. If one examines the Ni particles after oxidation and low temperature reduction in Fig. 3c carefully, it is evident that the original particles no longer have perfect shapes (cubooctahedra). Upon redisperssion, the particles break up into clusters of smaller crystallites. Many of them are very small. Because these smaller particles remain as clusters, the H_2 chemisorption increases but not as much as would be expected if the particles were isolated. The major difference in the uptake is due to the redispersion of particles into clusters of smaller crystallites rather than to totally separated perfect particles. It is clear that the change in particle morphology cannot be perfectly correlated with H_2 chemisorption. Only microscopy can see the individual particles and identify the morphology change. Supported metal particles are exposed to various oxidizing and reducing gas atmospheres during their preparation, operation and regeneration. It is reasonable that different treatments will alter the distribution of different crystallographic planes and affect the performance of the catalysts.

As shown in Figs. 1–3, oxidation–reduction cycles produce redispersion of Ni particles. Upon redispersion, the particles break up into clusters of smaller crystallites which have a larger fraction of corner and edge atoms on the surface. It is obvious that more high index planes were generated because of redispersion. Caracciolo and Schmidt (*27*) reported that the carbon deposition was lower on low index planes but higher on high index planes. The trend of decreasing methane turnover number with increasing dispersion (Fig. 3) is in agreement with the data of Bartholomew *et al.* (*13*) for Ni/SiO_2 catalysts and of Goodman (*20*) for Ni single crystals.

It has been demonstrated repeatedly that the activity and selectivity of catalysts depend on preparation techniques and pretreatments. The example described here shows that morphological changes in a single sample can be altered by sequential treatments. In Table 1, some of the TOFs of CO hydrogenation over Ni/SiO_2 catalysts reported in literature have been extrapolated to 258°C using the reported activation energies and the activities at other temperatures. As we can see, the TOFs range between 5.2 and 20.0 × 10^{-3} sec^{-1}. The TOFs measured in our laboratory for a single-catalyst sample range between 9.6 and 27.8 × 10^{-3} sec^{-1}, which bracket the values reported by nearly all other laboratories. Our results also suggest that the discrepancies between kinetics reported by other laboratories probably arise from morphological differences resulting from different treatments.

SUMMARY

In these experiments solid-state transformations caused by repeated oxidation–reduction produced a 40% increase of surface area, but the methanation activities de-

creased by a factor of 2. Reduction at higher temperatures produced a reversible increase in activity and sintering which could be restored by a repeated oxidation–reduction cycle.

TEM showed that redispersion breaks up the parent particles into clusters of smaller particles which have a higher fraction of high index planes but lower activity. The crystallographic anisotropies in carbon deposition on Ni under CO hydrogenation conditions explains the dependence of catalyst performance on pretreatment.

These results show that dispersion and microstructure are not simply related because all of these results are on rather large particles (4% dispersion, 250 Å average diameter). Oxidation–reduction treatment induces a breakup of the Ni polyhedra produced by high-temperature H_2 annealing into clusters of very small particles. The clusters evidently possess many edge, corner, and rough plane atoms, even though the particle size remains large.

These results suggest that fundamental information about structure effects on catalysis can be obtained only using multiple surface analysis techniques. Hydrogen chemisorption gives the surface area, while TEM examines different crystallographic structure and phases of small supported particles, and XPS yields the surface composition under reaction conditions.

We have postulated that the crystallographic variation of carbon formation (inactive multilayers on all but (111) and (100) planes of Ni) may explain this behavior. carbon deposition studies in the UHV reactor system confirm that initial deactivation coincides with graphite buildup. We shall describe these results in a later paper.

REFERENCES

1. Bonzel, H. P., and Kerbs, H. J., *Surf. Sci.* **117,** 639 (1982).
2. Kelley, R. D., and Goodman, D. W., *in* "The Chemical Physics of Solid Surfaces and Heterogeneous Catalysis" (D. A. King and D. P. Woodruff, Eds.), Vol. 4, p. 427. Elsevier, Amsterdam, 1982.
3. Mills, G. A., and Steffgen, F. W., *Catal. Rev.-Sci. Eng.* **8,** 159 (1973).
4. Vannice, M. A., *Catal. Rev.-Sci. Eng.* **14,** 153 (1976).
5. Ponec, V., *Catal. Rev.-Sci. Eng.* **18,** 151 (1978).
6. Biloen, P., and Sachtler, W. M. H., "Advances in Catalysis," Vol. 30, p. 165. Academic Press, New York, 1981.
7. Chen, J. J., and Ruckenstein, E., *J. Catal.* **69,** 254 (1981).
8. Baker, R. T. K., Prestridge, E. B., and Garten, R. L., *J. Catal.* **59,** 293 (1979).
9. Chen, M., and Schmidt, L. D., *J. Catal.* **55,** 348 (1978); **56,** 198 (1979); **60,** 356 (1979).
10. Wang, T., and Schmidt, L. D., *J. Catal.* **70,** 187 (1981); **71,** 411 (1981); **78,** 306 (1982).
11. Nakayama, T., Arai, M., and Nishiyama, Y., *J. Catal.* **79,** 497 (1983); **87,** 108 (1984).
12. Vannice, M. A., *J. Catal.* **40,** 129 (1975); **44,** 152 (1976).
13. Bartholomew, C. H., Pannell, R. B., and Butler, J. L., *J. Catal.* **65,** 335 (1980).
14. Dalla Betta, R. A., Piken, G. A., and Shelef, M., *J. Catal.* **35,** 54 (1974).
15. King, D. C., *J. Catal.* **51,** 386 (1978).
16. Kellner, C. S., and Bell, A. T., *J. Catal.* **75,** 251 (1982).
17. van Hardeveld, R., and Hartog, F., "Advances in Catalysis," Vol. 22, p. 75. Academic Press, New York, 1972.
18. Amelse, J. M., Schwartz, L. H., and Butt, J. B., *J. Catal.* **72,** 95 (1981).
19. Vannice, M. A., *J. Catal.* **50,** 228 (1977).
20. Goodman, D. W., Kelley, R. D., Madey, T. E., and Yates, J. T., Jr., *J. Catal.* **63,** 226 (1980); Kelley, R. D., and Goodman, D. W., *Surf. Sci.* **123,** L743 (1982).
21. Mullenberg, G. E., Ed., "Handbook of X-Ray Photoelectron Spectroscopy." Perkin–Elmer Press, 1978.
22. Shalvoy, R. B., Reucroft, P. J., and Davis, B. H., *J. Catal.* **56,** 336 (1979).
23. Krebs, H. J., Bonzel, H. P., and Gafner, G., *Surf. Sci.* **88,** 269 (1979); Bonzel, H. P., and Krebs, H. J., *Surf. Sci.* **91,** 499 (1980).
24. Sexton, B. A., and Somorjai, G. A., *J. Catal.* **46,** 167 (1977); Dwyer, D. J., and Somorjai, G. A., *J. Catal.* **52,** 291 (1978).
25. Erley, W., and Wagner, H., *Surf. Sci.* **74,** 333 (1978); Erley, W., Ibach, H., Lehwald, S., and Wagner, H., *Surf. Sci.* **83,** 585 (1979); Murayama, Z., Kojima, I., Miyazacki, E., and Yasumori, I., *Surf. Sci.* **118,** L281 (1982).
26. Gwathmey, A. T., and Cunningham, R. E., "Advances in Catalysis," Vol. 10, p. 57. Academic Press, New York, 1958.
27. Caracciolo, R., and Schmidt, L. D., *J. Vac. Sci. Technol. A* **2**(2), 995 (1984); *Applied Surface Science* **25,** 95 (1986).